resources

MDPI

Article

Hydrogeochemical Characterization as a Tool to Recognize "Masked Geothermal Waters" in Bahía Concepción, Mexico

Pablo Hernández-Morales [1], Jobst Wurl [2,*], Carlos Green-Ruiz [3,*] and Diego Morata [4]

1 Posgrado en Ciencias Marinas y Costeras, Universidad Autónoma de Baja California Sur, Carretera al Sur km 5.5, La Paz 23080, Mexico; phernandez_14@alu.uabcs.mx
2 Departamento Académico de Ciencias Marinas y Costeras, Universidad Autónoma de Baja California Sur, UABCS, Carretera al Sur km 5.5, La Paz 23080, Mexico
3 Unidad Académica Mazatlán, Instituto de Ciencias del Mar y Limnología, Universidad Nacional Autónoma de México, Av. Joel Montes Camarena s/n, Playa Sur, Mazatlán 82040, Mexico
4 Departamento de Geología y Centro de Excelencia en Geotermia de Los Andes (CEGA), Facultad de Ciencias Físicas y Matemáticas, Universidad de Chile, Plaza Ercilla 803, Santiago 8370450, Chile; dmorata@ing.uchile.cl
* Correspondence: jwurl@uabcs.mx (J.W.); cgreen@ola.icmyl.unam.mx (C.G.-R.)

Abstract: Geo-thermalism has been widely recognized on the Baja California Peninsula, especially during the last decade. The current research, carried out on Bahia Concepcion, evidences the existence of geothermal springs, which get recharged mainly by groundwater and seawater. The groundwater can be characterized as Na^+-Cl^- and Na^+-HCO_3^- type, with a pH value close to neutrality. The slightly more acidic thermal sites presented temperatures between 32 °C and 59 °C at the surface. Based on the relationships of the Cl^- and Br^-, as well as the B/Cl^-, and Br^-/Cl^- ratios, seawater was recognized as the main source of salinity. The spatial distribution is explained directly through marine intrusion, or via sprays and aerosols within the rainwater. Seawater ratios in thermal springs varied from 62% to 83%, corresponding mainly to shallow inflow, but seawater inputs into the deep thermal reservoir were also recognized. Temperatures in the geothermal deep reservoir were inferred from 114 to 209 °C, calculated through the SiO_2 and Na^+-K^+ geothermometers. In addition to previously reported thermal sites at Bahía Concepción, and based on their elevated temperatures, two new sites were identified. Another five springs do not fulfill the commonly used definition, based on differential temperature, but show the typical hydrogeochemical signature of thermal water. A new approach to identify this low-temperature geothermal-influenced spring water by its hydrogeochemical composition is presented, for which the term "Masked Geothermal Waters" (MGW) is introduced. Our findings increase the area of the geothermal anomaly and, therefore, the potential of geothermal resources. The approach proposed in this research will also be useful to identify more MGW in other coastal areas.

Keywords: Br^-/Cl^-; California Peninsula; thermal springs; mix water; seawater signature

Citation: Hernández-Morales, P.; Wurl, J.; Green-Ruiz, C.; Morata, D. Hydrogeochemical Characterization as a Tool to Recognize "Masked Geothermal Waters" in Bahía Concepción, Mexico. *Resources* **2021**, *10*, 23. https://doi.org/10.3390/resources10030023

Academic Editor: Elena Cristina Rada

Received: 1 January 2021
Accepted: 26 February 2021
Published: 4 March 2021

1. Introduction

Due to hydrocarbon deposit depletion, the need to reduce CO_2 release to the atmosphere, as well as international environmental agreements, renewable energies have largely escalated in importance in the world in becoming the future's energy resources, [1,2]. The environmental importance of these alternative energy sources has been recognized [3,4]. Although geo-thermalism is a renewable resource with a significant global occurrence, its use is still incipient compared to other alternative energies. However, derived from scientific and technological advances, which allow the reduction of operating costs, its future promises to be interesting, competing with other sources of energy [5]. Based on their usefulness, the research on geothermal resources has focused mainly on the assessment of high-temperature geothermal fields, leaving those of medium and low temperature at a second level of importance. In recent years, interest has increased in medium and

low-temperature geothermal sites, which can be used in small-scale power generation and other industrial activities that take direct advantage of the use of the geothermal fluid temperature [6].

Geothermal activity, manifested as low or high enthalpy thermal springs, is distributed throughout the world [7–9]. Due to its chemical characteristics, water from thermal springs has been used historically in balneology, balneotherapy, traditional medicine and more recently in the cosmetic or food industries [10–12]. However, several studies recognize the release of nutrients and potentially toxic elements from the discharge of thermal water into the environment [13–18].

The widely accepted definition for recognizing a water spring as thermal is based on its differential temperature values, compared with the average annual temperature in the respective area [19,20]. Groundwater chemical composition is an important aspect to understand the hydro-thermalism, as several springs do not show the mentioned differential, but their hydrogeochemical signature suggests a hydrothermal origin. Authors herein propose to define these kinds of waters as masked geothermal waters (MGW). In this context, the study of water mixtures of thermal fluids, groundwater and seawater [13,21–25] allows us to recognize origin of fluids, groundwater discharges, marine intrusion, movement of the saline interface, and coastal ecosystem relationship and vulnerability. Knowing these mechanisms allows for better resource management [22,25–27].

In Mexico, geothermal resources have been used as a source of energy production since the middle of the 20th century. In 2018, an estimated 5375 GWh were produced from high-enthalpy geothermal fields such as Los Azufres, Los Humeros, Cerro Prieto, and Las Tres Vírgenes (LTV), which represents 1.7% of electrical national production [28,29]. The last two of these fields are located on the Baja California Peninsula (BCP). As a result of recognizing the high potential and heat flow prevailing in this area, including in the Gulf of California [6,30,31], several low and medium-temperature geothermal manifestations have been located and related to volcanic activity or/and fractured areas (regional faults), but not fully characterized from a hydrogeochemical point of view. In particular, on the southern portion of the peninsula, corresponding to the Baja California Sur State, geothermal sites have been described [6,32–38]. These manifestations are located mainly on the eastern margin of the BCP, discharging into the Gulf, and Bahía Concepción is one of the most important [6,36,39–41].

The aim of this study was to describe geothermal manifestations in Bahia Concepcion and to identify their effects on groundwater geochemistry. Additionally, a new methodology based on hydrogeochemical signatures is proposed to recognize MGW. A hydrogeochemical characterization of the groundwater that discharges into the bay was performed to clarify the exchange and mixing of the fluid endmembers in the MGW. The information generated in this research contributes to an increase in knowledge on geothermal resources for their future use and management in a sustainable framework.

2. Study Area

Bahía Concepción, located in the central-eastern portion of B. C. S. (Figure 1), is an area with a low population density. Its natural landscape's beauty has made it a tourist destination, with future development projections, which implies the need for energy and water resources. The area has good accessibility and the most important settlements are: Santispac, El Burro, Rancho El Molino, Punta Arenas, El Coyote, La Posada, all on the west coast of the Bay (Figure 1).

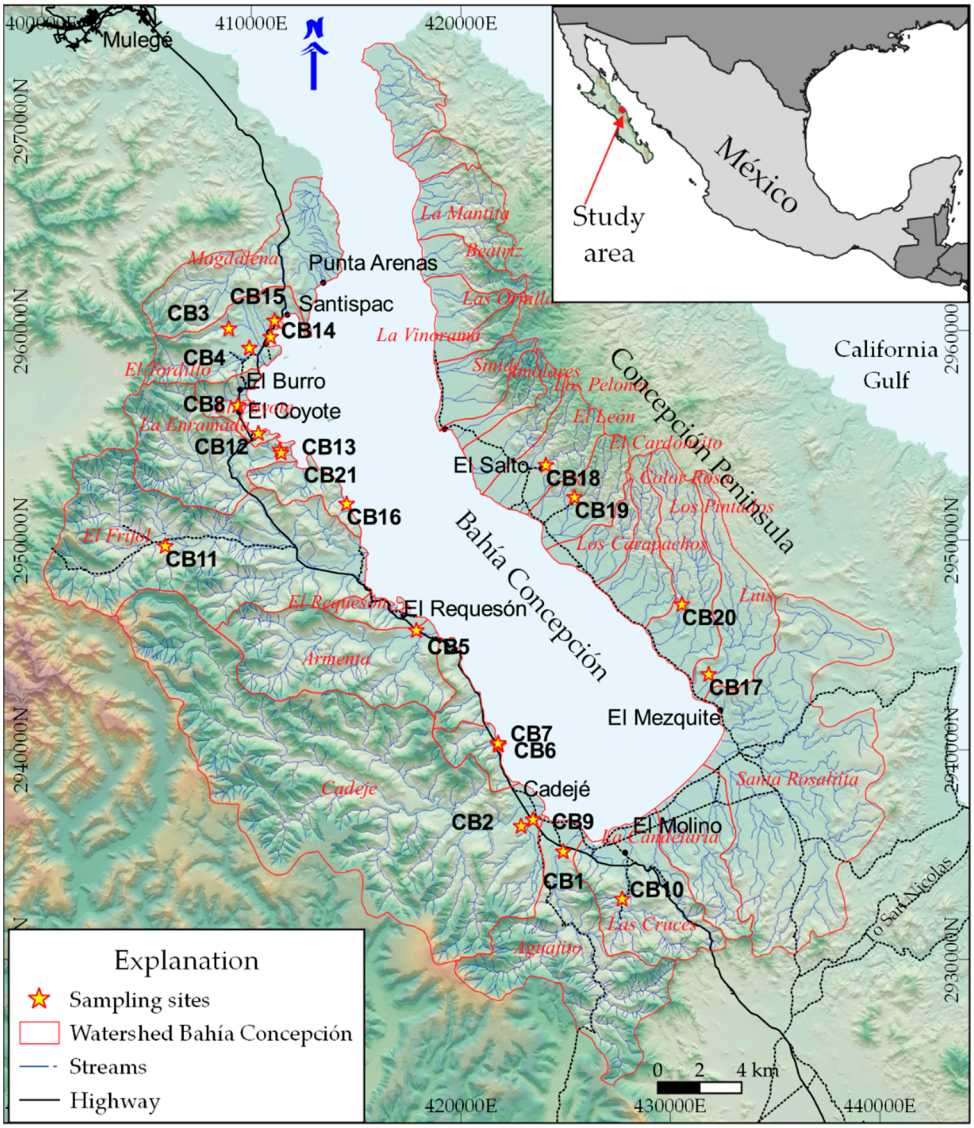

Figure 1. Study area at Bahía Concepción and sampling sites.

2.1. Geological Units

The oldest unit outcropping on the Bahia Concepción region corresponds to cretaceous granitic rocks (Figure 2), with inclusions and pendants of schists, intruded by mafic, aplitic, and pegmatitic stocks and dikes [42,43]. The El Salto Formation (28.1 ± 09 Ma), discordant to that granitic basement, was formed by very fine to medium grain sandstones with cross-bedding stratification and tuffaceous intercalations [43].

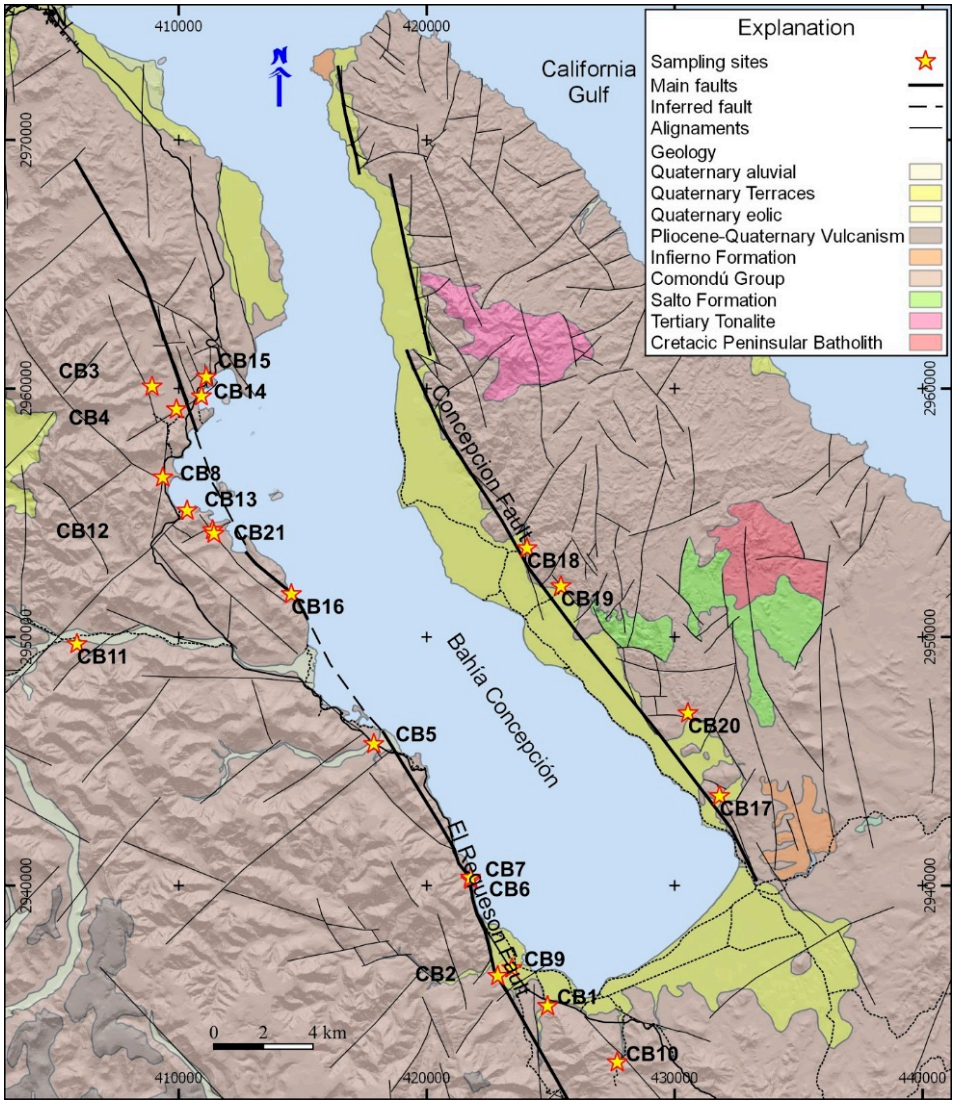

Figure 2. Geological and structural generalized map of Bahia Concepción area. Modified from McFall [43], SGM [44], Ledesma-Vázquez and Johnson [45].

It is transitionally overlaid by rocks of the Comondú Group [43,46,47] volcano-sedimentary sequence (Figure 2). Umhoefer et al. [47] proposed three divisions: (1) a lower clastic unit with sandstones and tuffaceous intercalations, (2) a middle unit with volcanic breccias and dacitic-andesitic lava flows and (3) an upper unit of lava flows. The Comondú Group was deposited ca. 30 Ma–12 Ma [46–48]. In a transitional to discordant contact with the Comondú Group, the Infierno Formation, is overlaid composed of andesitic conglomerates, sandstones, siltstones, mudstones, and coquina intercalations, with a characteristic chert layer [49,50]. The Infierno Formation from the Upper Pliocene is deposited in a beach environment with marine transgression [43,49]. Lava flows and volcanic deposits overlay the previous units, identified as andesitic-basaltic alkaline to rhyolitic-dacitic calco-alkaline post-Comondú [51–53]. Alluvial deposits fill the dry stream, sands and heterogeneous conglomerates compose terraces at different levels associated with the structural system, as well as dune deposits, which currently make up the geomorphology of the coastal zone in the area.

2.2. Structural Setting

The structural genesis of Bahía Concepción is closely related to the events that occurred at the initial spreading of the Gulf of California in the late Miocene [45,48,52,54].

During the Cenozoic, the processes of a convergent margin ceased, originating an arc, whose volcanism (sensu lato) produced the Comondú Group deposits [42,55]. After the subduction, a trans-tensional process began, which would merge the Baja California peninsula as part of the Pacific plate [48,56]. The current boundary between the Pacific Plate and the North American plate, along with the GC, corresponds to an oblique (20° NW) transform fault [54].

The major structures in Bahía Concepción correspond to normal faults with associated listric structures (Figure 2) with a preferential direction 25–30° NW–SE, while secondary alignments are perpendicular NE–SW (Figure 2). The Concepción Fault is the main structure on the Concepcion peninsula which exhibits a general dip of 45° to the west [43,52]. A second structure (NW–SE) is the El Requesón Fault (Figure 2), which delimits the western margin of the bay where intertidal and submarine hydrothermal springs occur [57]. These two structures formed a graben, which corresponds to Bahía Concepción bay. Faulting is considered to completely affect the volcano-sedimentary sequence, probably as well as the intrusive igneous basement which can be considered almost impermeable. As the structural system of the area is related to the opening of the California Gulf, the main faults and their associated structures allow a relatively high permeability. The intensive faulting can explain the existence of deep circulation in the aquifers, which has been described as the main source of the geothermal system.

2.3. Climate and Hydrogeology

The climate in Bahía Concepción is semi-arid. Based on data from three meteorological stations [12], the time series of monthly records for 25 years indicates that the average annual precipitation is 145 mm, less than the average precipitation of the State (222 mm) [58]. The annual average temperature is approximately 23 °C (Table 1).

Table 1. Annual averages of precipitation (mm) and temperature (°C) in Bahia Concepcion [59].

Parameter	Meteorological Station			Local Average in Bahia Concepción
	San Nicolás	Mulegé	Ojo de Agua	
Annual precipitation average (1980–2015)	142.3	153.6	141.8	145.9
Annual temperature average (1980–2015)	23.73	22.31	22.37	22.80

The drainage pattern in the area is dendritic and subparallel. The main creeks at the western side of the bay are Cadeje, Armenta, El Frijol, La Enramada, and El Tordillo; while Los Pelones, El León, Cardoncito, Los Pintados, and El Mono-Santa Rosaliíta creeks drain to the east coast of the bay.

For Bahia Concepcion watershed, including the aquifer, the Mexican National Water Commission (CONAGUA) calculated an average annual recharge of 5.7 Mm^3; in contrast, the average annual discharge reaches approximately 4.9 Mm^3 [60]. These numbers include the San Nicolás watershed, which discharges directly towards the Gulf of California and not towards the bay, thus the discharge into the bay is assumed to be lower than calculated. CONAGUA indicated that the aquifer is formed by the volcano-sedimentary rocks in the area [60]. These rocks, mostly, belong to the Comondú Group, according to the geology of the area (Figure 2). In the aquifer, a transmissivity of 0.5 to 3.5 $\times$ 10^{-3} m^2/s was estimated. The depth of the water table varies between 1 to 20 m, obtained from wells in dry streams and near to the coastline, which is defined as the discharge area of the aquifer. Regarding to elevation of the water table, this was measured up to 230 m.a.s.l., towards the mountainous area [60].

2.4. Geothermal Research in the Area

Former investigations, related to the geothermal system in Bahía Concepción, are mainly focused on the submarine discharges of thermal water and intertidal thermal

springs, located near Santispac and Mapachitos [36]. Water composition of two intertidal thermal springs (Santispac and La Posada), as well as a submarine hot spring (Mapachitos), was described as a mixture of seawater and thermal fresh groundwater. These thermal springs are enriched in several elements, but depleted in Mg, with respect to seawater [32,36]. The temperature in the deep reservoir was calculated at about 200 °C [36]. A high heat flux (up to 200 mW/m^2) is concentrated in this region [53]. The geothermal system was defined as controlled by deep normal faults, associated with the oblique extensional system of the Gulf of California [36,39,61].

Villanueva-Estrada et al. [41] used data from Prol-Ledesma et al. [36] and proposed a mixing model that explains the final fluid discharge. They concluded that the water source of the thermal system is meteoric water (80%) and the remaining 20% represents high saline fluids. Elements such as Mn, Ba, Hg, and Si occur in the areas of submarine thermal discharges, as well as at the intertidal springs. The elevated concentrations of As and Hg, among other potentially toxic elements, were related to the discharges of the intertidal hydrothermal spring of Santispac and Mapachitos; these elements are found to be assimilated by macroalgae [40,62]. Estradas-Romero et al. [63] and Melwani and Kim [64] related species richness of phytoplankton and benthic fauna to higher water temperature and the hydrogeochemical composition of thermal discharges.

3. Methods

In February 2018, seven groundwater (hand-dug shallow wells, called norias) and 13 spring water samples were collected from the coastal margins of Bahía Concepción, following the recommendations of Arnórsson and D'Amore [65]. The samples from wells were taken with a bailer, avoiding shaking and contamination. In the case of springs, the sample was taken directly from the emanation point. All samples were filtered with a 0.45 µm cellulose Millipore® filter (Merkmillipore, Burlington, MA, USA) and stored in new polyethylene bottles previously rinsed with distilled water, and again with water from the source to be sampled. Finally, the samples for cation analyses were acidified with HNO_3 (pH < 2) (J.T. Baker®-Avantor, Center Valley, PA, USA), and all samples were stored at 4 °C until analysis.

At each site, three physicochemical parameters were measured: firstly, the temperature, using a pH/temperature meter (Hanna Instruments® HI9124; Woonsocket, RI, USA) with a resolution of 0.1 °C and an accuracy of 0.4 °C. The electrical conductivity (EC), as well as the total dissolved solid (TDS) were measured by a CE/TDS/temperature DiST® 6 m (Hanna Instruments® HI98312; Woonsocket, RI, USA) with temperature compensation, and detection ranges of up to 20,000 µS/cm and up to 10 ppt, respectively. The resolution and accuracy of this device are 10 µS/cm and ±2% for EC and 0.01 ppt and ±2% for TDS. For sites with high salinity, a portable refractometer was used to measure the percentage content of salts in UPS. The pH was also measured, using the Hanna Instruments® meter, HI9124 (Woonsocket, RI, USA), with resolution of 0.01 and an accuracy of ±0.01. It was previously calibrated, using Buffer solutions (4.01, 7.01, 10.01 Hanna®; Woonsocket, RI, USA). The main cations (Ca^{2+}, Na^{+}, K^{+}, Mg^{2+}) were determined with a Perkin Elmer® (Waltham, MA, USA) PinAAcle 900F Flame Atomic Absorption Spectrophotometer (recovery 101%, 102%, 96%, 102% and limits of detection -LOD- 0.02, 0.03, 0.12, 0.02 mg/L, respectively). The major anions (Cl^{-}, $SO_4{}^{2-}$, Br^{-}) were analyzed in a Metrohm® (Herisau, Switzerland) Ion Chromatograph model 861 Advanced Compact IC (recovery of 95%, 107%, 104% and LOD 0.01, 0.03, 0.02 mg/L, respectively). These analyses were validated (±5%), calculating the charge balance of the major cations and anions for each sample. The elemental concentration of B (recovery 94%, LOD 0.07 µg/L) was determined by mass spectrometry using a Thermo Scientific® (Waltham, MA, USA) ICP-MS iCAP Q equipment. The concentration of $HCO_3{}^{-}$ was determined by automatic titration with a Hanna® HI-902C (Woonsocket, RI, USA) equipment. SiO_2 was analyzed with a Hanna® photometer (±0.03 mg/L) (Woonsocket, RI, USA). All the analyzes were validated using control reference solutions and NIST-1643f as certified reference material. For quality control, laboratory

and field blanks were also analyzed and no chemical interferences (sample contamination) were found.

According to Vengosh [66], the Br^-/Cl^- and B/Cl^- relationships allow the recognition of the mixing effects of thermal water with seawater, evaporated seawater, fresh groundwater, or agricultural return flow. Hernandez-Morales and Wurl [34] used the diagram proposed by Vengosh [66], to define typical positions of thermal water at the southern tip of the peninsula of Baja California Sur. The origin of the salinity in the study area is discussed based on Cl^-, Br, and B relationships.

The temperature in the deep thermal reservoir was inferred using the silica geothermometer [67] with the SOLGeo software [68], which allows estimation of the uncertainties for the incorporated geothermometric equations.

4. Results

The physicochemical results measured in the field indicated that the water from the sampling sites had temperatures ranging from 22 °C (CB12) to almost 60 °C in the coastal thermal springs (CB14, CB15, and CB16, Figure 1). The sites CB2 (Cadejé) and CB3 (El Tordillo) showed a temperature above 32 °C and therefore fall into the definition of thermal water, considering the average temperature of the area (22.8 °C). The temperature was higher on the slope that discharges into the west of the bay. Temperature, electrical conductivity and pH had a greater variability on the western margin of the bay, due to the occurrence of geo-thermalism and a stronger seawater influence. The eastern margin (CB17, CB18, CB19, and CB20) showed electrical conductivities from 1082 to 2130 µS/cm, with a pH average of 6.9. The sampling sites on the western portion (Figure 1) showed high values of electrical conductivity for the sites near the coast, in contrast to the sites upstream of the hydrological watershed; a variation was found from 430 µS/cm (CB11) to greater than 20,000 µS/cm in coastal thermal springs (CB14, CB15, CB16). Regarding the pH of the coastal thermal springs, slightly more acidic values (pH 6.5) were found than the values registered in the samples of the other analyzed sites, which varied from a neutral pH to 8.7 (CB10). Detailed information is presented in Tables 2 and 3.

Table 2. Sampling sites code and physicochemical parameters.

Sample	Locality	Electric Conductivity (µS/cm)	TDS (mg/L)	Salinity (UPS)	Temperature (°C)	pH
		Western margin				
CB1	Casa de Piedra	981	698	–	27.4	7.7
CB2	Cadejé	1160	506	–	36.4	8.2
CB3	El Tordillo	8300	4069	–	32.7	7.7
CB4	El Llanito	15,720	9133	–	28.8	6.5
CB5	Armenta	737	384	–	25.8	7.2
CB6	Pocitos 2	4446	3231	–	23.6	7.5
CB7	Pocitos 3	8160	6440	–	30.3	7.3
CB8	Predio Adelaido	6070	3014	–	29.4	7.3
CB9	Arroyo Cadejé	4020	2571	–	27	7.3
CB10	Las Cruces	1779	1143	–	22.8	8.7
CB11	Las Cuevitas	490	358	–	30.7	7.9
CB12	La Enramada	949	741	–	22.2	8.1
CB13	El Coyote	4660	3442	–	31.6	7.2
CB14	La Posada	>20,000	25,942	22	53.4	6.9
CB15	Santispac	>20,000	29,320	25	42.1	7.8
CB16	Agua Caliente	>20,000	24,214	21	58.6	6.5
CB21	Santa Barbara	4960	3167	–	30.4	7.2
		Eastern margin				
CB17	El Mezquite	2130	1338	–	29.8	6.7
CB18	El Salto	1135	675	–	24.3	6.9
CB19	McFall	1082	653	–	24.7	6.9
CB20	La Pintada	1161	755	–	23.2	6.9

Most of the analyzed samples indicate Cl^- and $HCO_3{}^-$ as dominant anions. Only for CB19 was the dominant anion $SO_4{}^{2-}$. Regarding cations, a higher concentration of Na^+

prevails in all samples. In addition, the results indicated high concentrations of Na^+ and Cl^-, with values up to 17,629 and 8150 mg/L, respectively, for the CB15 sample. On the contrary, the lowest concentration in Na^+ and Cl^- (53.6 and 44.5 mg/L) corresponded to the CB11 sample.

Table 3. Hydrogeochemical composition of the samples collected in the Bahía Concepción area. Units are in mg/L.

Sample	Na^+	K^+	Ca^{2+}	Mg^{2+}	Cl^-	SO_4^{2-}	HCO_3^-	Br^-	B	SiO_2	Electrical Balance Error (%)
Western margin											
CB1	148.0	3.6	26.2	26.1	164.7	24.8	285.0	0.5	0.6	42.3	−1.2
CB2	112.0	4.5	26.4	14.8	130.9	27.6	162.8	0.5	0.5	78.8	0.6
CB3	615.0	32.4	434.0	235.5	2391.9	166.2	152.0	8.4	0.7	121.6	−3.8
CB4	1590.0	74.2	807.0	494.0	5472.6	414.5	231.0	18.4	1.4	129.5	−4.9
CB5	67.0	9.4	23.5	10.4	64.9	10.0	197.8	0.2	0.1	43.0	−1.1
CB6	900.0	26.0	54.8	108.0	1653.5	237.6	234.0	5.4	0.7	77.8	−4.0
CB7	1900.0	68.9	112.0	204.6	3397.0	460.4	278.7	11.2	1.0	103.0	−1.6
CB8	600.0	33.4	180.4	167.0	1659.6	212.3	122.9	5.6	0.8	53.0	−4.0
CB9	845.0	22.2	7.1	20.8	977.1	167.9	482.9	3.2	1.3	64.6	−1.5
CB10	320.0	6.3	20.6	23.0	338.9	103.3	312.7	1.3	8.4	83.1	−0.9
CB11	44.5	4.0	21.8	22.6	53.6	11.1	170.9	0.3	0.1	80.0	−1.2
CB12	120.2	36.1	26.1	30.7	142.3	15.1	356.1	0.7	0.3	63.2	−3.2
CB13	735.0	30.3	158.0	200.8	1943.1	216.6	127.3	6.5	0.5	72.7	−4.0
CB14	7225.0	446.3	1229.5	404.0	15,620.4	946.8	70.4	52.6	8.7	75.1	−4.7
CB15	8150.0	455.4	1271.0	519.0	17,629.5	1213.4	81.6	59.9	7.6	78.8	−5.2
CB16	7100.0	521.1	1092.5	276.0	14,585.9	495.0	143.3	51.1	15.4	211.7	−3.0
CB21	717.5	28.3	110.0	174.0	1757.3	197.0	150.9	5.9	0.4	72.0	−4.6
Eastern margin											
CB17	395.0	4.8	34.5	18.0	388.3	57.6	428.3	1.4	0.4	66.4	2.9
CB18	142.0	1.1	52.7	13.0	143.8	182.9	127.9	0.4	0.3	44.2	−1.2
CB19	109.0	0.6	74.6	14.9	93.8	170.7	165.4	0.3	0.2	44.4	2.1
CB20	140.0	2.3	70.6	18.4	182.0	23.7	307.4	0.6	0.2	40.6	1.6

Based on the concentration of the major ions, hydrogeochemical facies can be generalized according to Piper's diagram [69,70]. The hydrogeochemical classification of the analyzed sites in this work resulted in Na^+-HCO_3^- type waters in the area with contribution mostly of fresh groundwater (CB1, CB2, CB5, CB10, CB11, CB12, CB17, CB20); while, in the sites near the coastal zone the type of water is Na^+-Cl^- (CB3, CB4, CB6, CB7, CB8, CB9, CB13, CB14, CB15, CB16, CB21). Sites CB18 and CB19, located on the central portion of the Concepción Peninsula, belong to a Na^+-SO_4^{2-} water type. The Piper diagram (Figure 3) exhibits two main groups of waters, group 1 that enclose samples related to seawater reference and group 2, in the central part of the rhomboid, with less mineralization and bicarbonate-sodium type. The average concentration of anions and cations for both groups, from highest to lowest, is as follows: (1) $Cl^- > SO_4^{2-} > HCO_3^- > Br^-$; $Na^+ > Ca^{2+} > Mg^{2+} > K^+$. (2) $HCO_3^- > Cl^- > SO_4^{2-} > Br^-$; $Na^+ > Ca^{2+} > Mg^{2+} > K^+$.

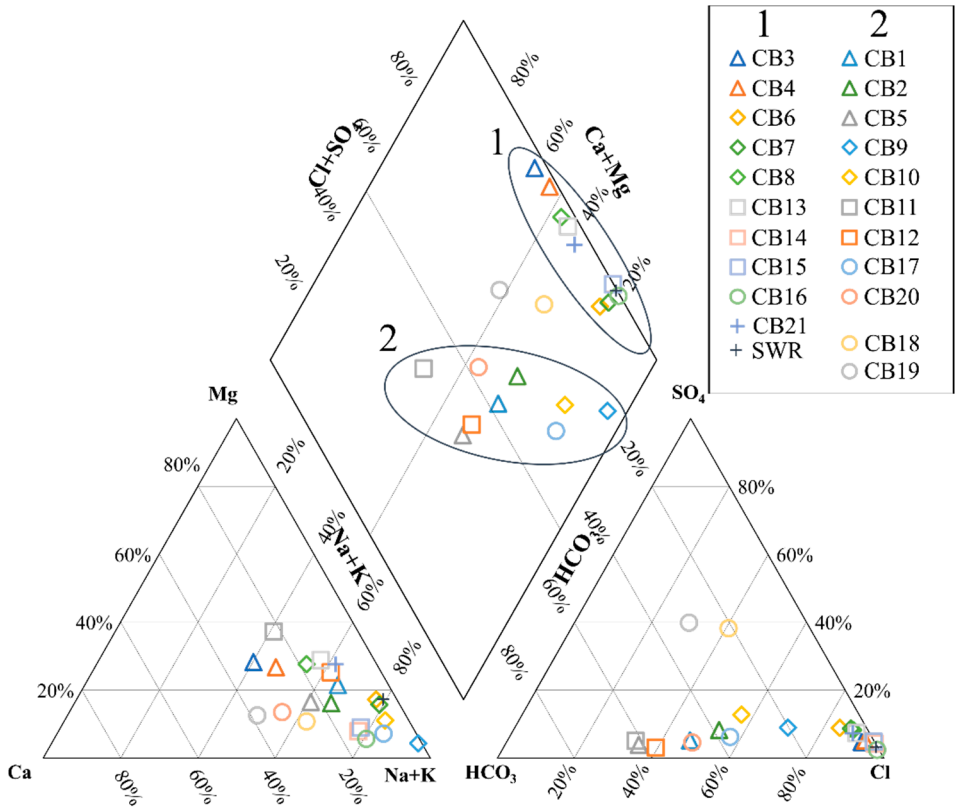

Figure 3. Classification of groundwater from Bahía Concepción, according to the Piper diagram.

Hydrogeochemical Characterization

The Santispac, La Posada, and Agua Caliente (CB14, CB15, CB16) localities, with a salinity greater than 21 PSU and temperature up to 50 °C, correspond to intertidal thermal springs and have been described as mixtures of thermal water and seawater [36,41]. This is in agreement with our results (Table 1). The samples CB1, CB5, CB11, CB12, and those located on the Concepcion Peninsula, presented lower mineralization. The site CB11 (Cuevitas) has a similar hydrogeochemical signature as that described by Birkle et al. [71], as meteoric recharge water for the Las Tres Vírgenes geothermal field (ca. 100 km northwest). A slight SO_4^{2-} enrichment was found in samples CB18 and CB19 respecting their other anions; this is probably added from a mineral alteration of a tertiary igneous intrusion [48] occurring in that area (Figure 2).

Most of the sites fall into the region of alkali dominance in the Piper diagram (Figure 3). This is in accordance with the occurrence of alkaline to calco-alkaline volcanic and volcanoclastic rocks from the Comondú Group (Figure 2) in the area [46,55], indicating a probable water–rock interaction process. Two groups of samples are recognized from the Piper diagram. Group (1) on the upper right, with high contents of chloride, is formed by sites located near the west coastline (Figure 4); they show a trend in the direction of the decrease or exchange of Na^+ and this is associated with a mixture of seawater (SWR) and fresh groundwater. The second group on the central portion represents fresh groundwater and includes the site CB11, which shows an ionic composition commonly considered as recharge water. The sites belonging to this group are further from the coastline than those from group 1 (Figure 4), which could indicate a spatial evolution, as suggested Tomaszkiewicz et al. [72], based on the water mineralization from the recharge zone towards the coastline, where it acquires higher mineralization.

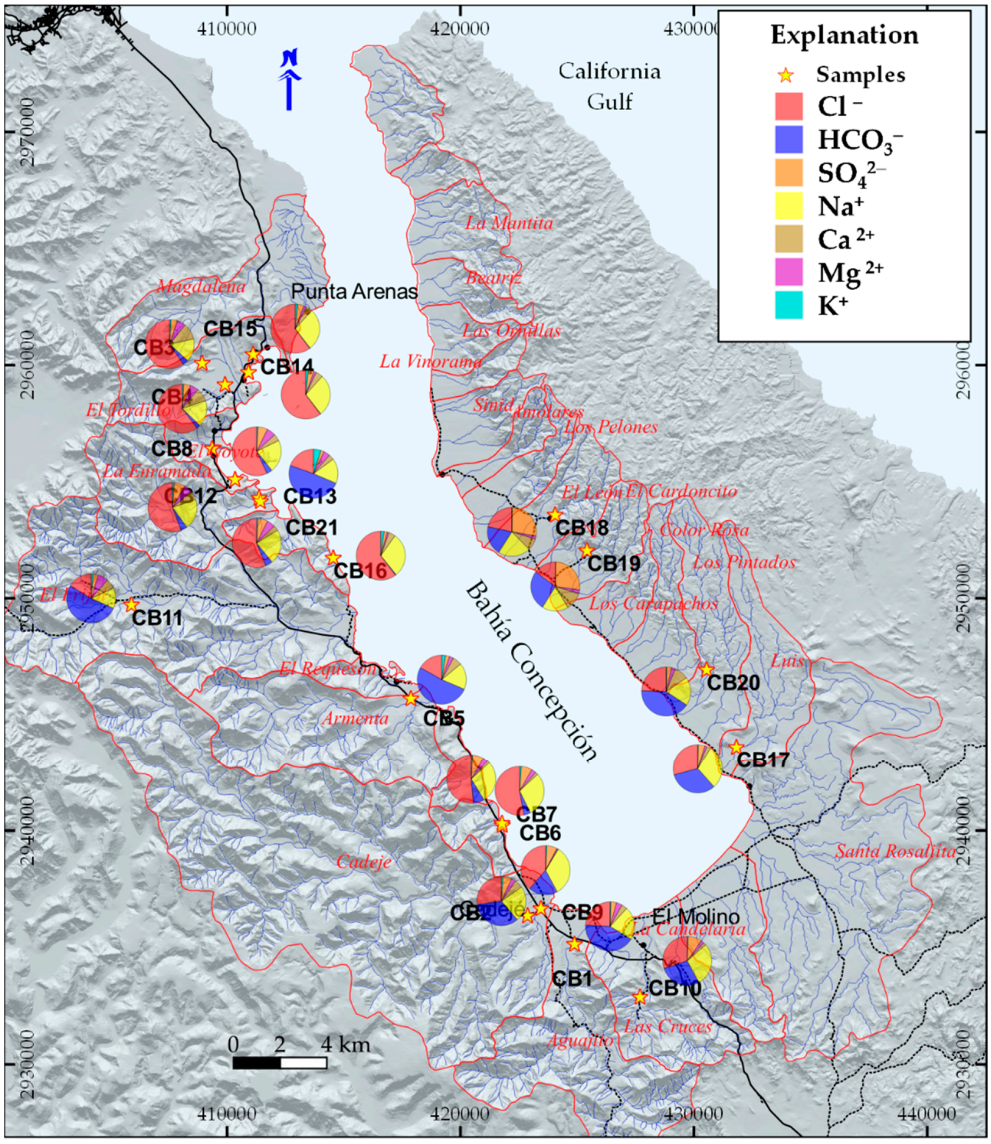

Figure 4. Spatial distribution of ionic concentration ratios.

The Br^{-}–Cl^{-} relationship maintained as constant, and similar to the relation from the seawater reference; although, for some sites, the Cl^{-} concentration is as low as that for meteoric water, following a common mixing pattern (Figure 5). Similarly, most of the samples maintain the seawater B–Cl^{-} ratio, except the sites CB10, CB14, CB15, CB16, with elevated boron concentration (Figure 5). In addition, the last three sites also showed lower Mg^{2+} ratios than seawater.

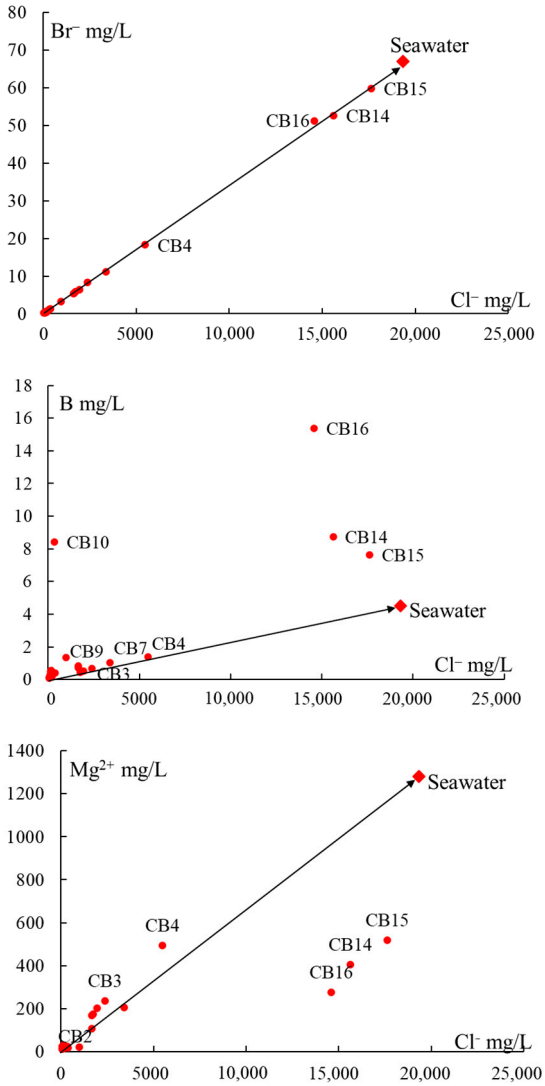

Figure 5. Relationships between Cl^- vs. Br^-, B and Mg^{2+} in groundwater from Bahía Concepcion watershed. Seawater data after Nozaki [73].

5. Discussion

Based on the Br^-–Cl^- relationship (Figure 5), a theoretical dilution line (Figure 6) was modeled between the two end-members (recharge freshwater represented by CB11 and seawater SWR), using the PHREEQC software [74]. According to the percentage of SWR, three groups are well distinguished:

(1) The samples CB14, CB15, and CB16, with more than 75% of seawater, correspond to the intertidal hydrothermal springs in La Posada, Santispac, and Agua Caliente (Figure 1).

(2) Three sites, located within the intertidal area (CB6, CB7, CB13), and five sites, located within a distance of less than 3 km to the coastline (CB3, CB4, CB8, CB9, and CB21), presented a fraction of seawater ranging between 5% and 30%. This proportion of seawater results from either tidal pump or groundwater extraction.

(3) The remaining sites, with less than 2% seawater, are located at distances of more than 3 km to the coastline.

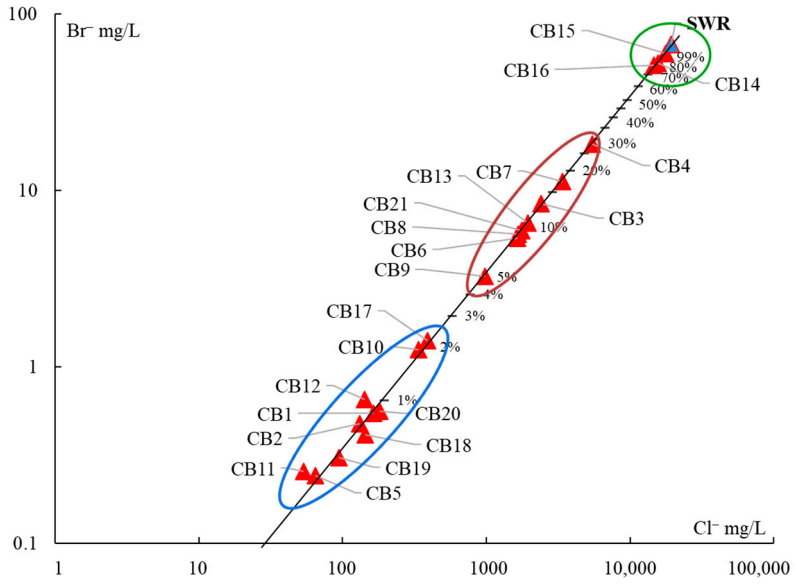

Figure 6. Cl^- and Br^- relationship with the samples analyzed, respecting the theoretical dilution line of seawater (SWR).

The probable addition of the seawater signature respecting its Br^-–Cl^- relationship would be explained by aerosols and spray particles added in the recharge from meteoric rainwater as explained for thermal springs at the southern tip of BCP [34]. The low percentage of seawater fraction in those sites could be an indicator of this process (Figure 6). With no storms or hurricanes occurring, marine aerosols can be recognized up to 20 km inland. Conversely a higher transport of marine spray and aerosols is expected in the rainy season which are mixed with the recharge meteoric water [75–77]. At Bahía Concepción, the rains are associated with hurricanes and storms and represent the main source of recharge [78].

5.1. Origin of Water Salinity and Mixing of End Members

The hydrogeochemical compositions of four end-members were defined as follows: (a) seawater [73], (b) meteoric recharged groundwater (CB11), (c) thermal water with meteoric water recharge [34], and (d) thermal water from the geothermal field LTV (LV4) [79]. The proportion of each end-member in the water samples was evaluated, based on the elements Cl^-, Br^-, and B, which represent conservative ions [67,80]. According to Vengosh [66], the relationship between Br^-/Cl^- and B/Cl^- ratios allows the recognition of mixtures of water. This relationship has been widely used in former studies on hydrothermalism in several countries [9,34,81–83].

All data from samples from Bahia Concepcion, as well as those from the known end-members, were plotted in the modified Vengosh diagram (Figure 7). The sites, including the thermal intertidal ones, maintained a Br^-/Cl^- ratio similar to that from the seawater reference; however, the B/Cl^- ratio remarkable varied among samples, oscillating from 0.0008 up to 0.08 (Figure 7). This can be explained by thermal water-rock interaction processes, providing a considerable increase in boron concentrations [84,85]. In the case of seawater evaporation, both ratios (Br^-/Cl^- and B/Cl^-) vary systematically, indicated in Figure 7 by a blue arrow. This effect is notable in the Mapachitos site from Bahía Concepción (BC1) described by Prol-Ledesma et al. [36]; however, in this study this was not observed.

The black diagonal arrows, parallel to the blue arrow, correspond to the trend of the Br^-/Cl^- and B/Cl^- ratios that has been described for hydrothermal manifestations of the Los Cabos Block [34], a mountain range in the center of the southern tip of the peninsula of Baja California. The thermal springs at El Chorro and Buenavista [34] are taken here as references (Figure 7).

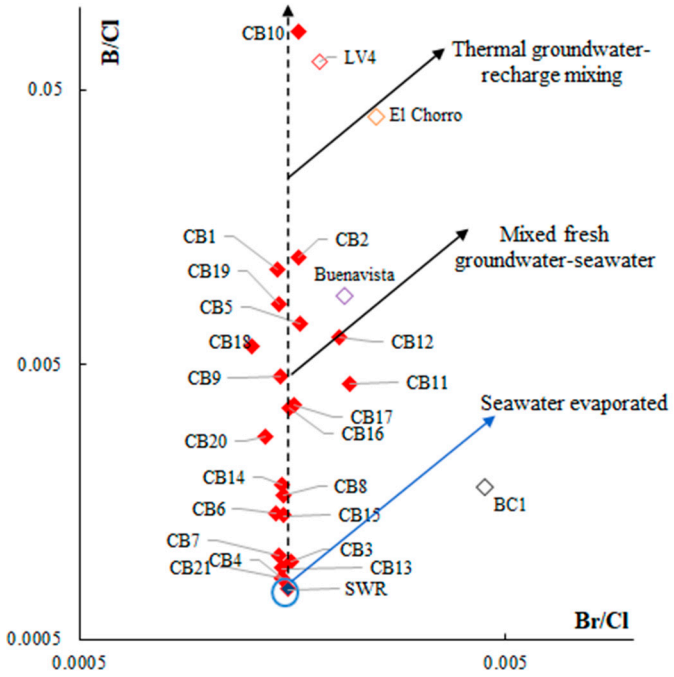

Figure 7. Br^-/Cl^- and B/Cl^- relationship for samples and end-members Data for seawater, LV4 (LTV), Buenavista, El Chorro, and BC1 were taken from [34,36,66,79], respectively.

According to the Br^-/Cl^- and B/Cl^- relationship (Figure 7), trend lines are projected in the same direction for evaporated seawater, as defined by Vengosh [66]. There is a contribution of marine waters from recharge, subsequently mixed either with a geothermal member or/and seawater. In the case of mixing with thermal water with meteoric recharge, samples tend to shift from the seawater Br^-/Cl^- ratio (dashed line, Figure 7), towards an increase of the Br^-/Cl^- and B/Cl^- ratios as in the case of the LV4, El Chorro and BC1. The relationship between the conservative Br, and Cl^- in the geothermal system of Bahia Concepcion maintains the common seawater molar ratio of 0.0015 [75,84,86], which rejects that the water in the aquifer has interaction with brines or strata with relict seawater, as has been indicated for sedimentary basins in China, U.S. and Poland [82,83,87,88]. B/Cl^- ratio varies with respect to seawater. Elevated boron concentrations are common in thermal studies [66,87], since this element is adsorbed by oxides or clay minerals and can be released into the water due to changes in temperature. Stefánsson et al. [84] indicate that low temperature thermal waters increase their B/Cl^- ratios, almost reaching the common ratio for basalts (0.017), upon progressive leaching processes during water–host rock interaction.

Birkle et al. [71] used a logarithmic scale to represent the Br^- and Cl^- relationship between the mixture of meteoric water and seawater (Figure 8). It is observed that the Las Tres Vírgenes thermal fluids are close to the relationship of seawater, inferring a direct mixture of marine water with groundwater recharge. In contrast, on the Br^-/Cl^- vs. B/Cl^- diagram [66], the sample LV4 is located close to the field defined as thermal water. Birkle et al. [71] described meteoric recharge as the main source. For LV4, the Br^-/Cl^- ratio similar to that of seawater also probably results from meteoric recharge, as indicated for the Bahía Concepción thermal sites, and would not correspond to a mixture with seawater in-depth (Figure 8). All samples maintain the Br^-/Cl^- ratio of seawater (Figures 7 and 8), however, the B/Cl^- ratio above 0.007 is a strong indicator to recognize MGW, considering anthropogenic inputs of boron in the area are negligible.

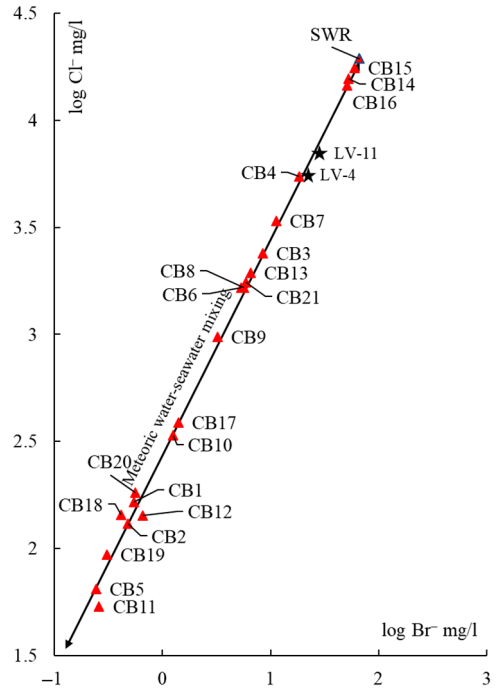

Figure 8. Diagram of log Cl^- and log Br^- showing samples from Bahía Concepción. LV-11 and LV-4 corresponding to the Las Tres Vírgenes (LTV) geothermal water in depth [71,79].

5.2. Masked Geothermal Water (MGW)

The temperatures of the intertidal thermal springs (CB14, CB15, and CB16) were measured at around 58 °C in February 2018, and similar temperatures were reported previously [36,40,41], indicating only little temporal variations. The temperature at the sites CB2, CB3, CB7, CB8, CB11, CB13, CB17, and CB21 (Table 1) varied from 29.4 to 36 °C (6 to 12 °C above the annual average for the area), which corresponds to the common definition of geothermal sites (according to the annual average temperature), but their hydrogeochemical composition also supports this finding, particularly B, Mg^{2+} and SiO_2 (Table 1).

The thermal springs CB14, CB15, and CB16 are closely related to seawater (more than 90%) and to the thermal end-member (Figure 8). The second group of samples (CB3, CB4, CB6, CB7, CB8, CB13, and CB21) are in the mixing zone between SWR and recharge, indicated by a depletion in Br^- from freshwater. The sites for CB3, CB6, CB7, and CB8 represent a subgroup, where an increase in B/Cl^- ratio indicates mixing with thermal water. Recharge of meteoric water explains most of the salinity for the rest of the sites (CB1, CB2, CB5, CB9, CB12, CB18, and CB19), mixed with a very low portion of other fluids (seawater fraction, (Table 4) and/or with the thermal end-member). As indicated by the Br^-/Cl^-–B/Cl^- diagram (Figure 7) and B/Cl^--Br^- (Figure 9), recharge water is introduced to the aquifer with a proportion of seawater through aerosols. The sites CB2 and CB3 show a geothermal influence that has not been described before. These sites can be related to different mixing portions (Figures 6 and 9), where CB2 is very close to the recharge water (Figure 9) and the thermal end-member, and El Tordillo CB3 results from mixing with seawater due to seawater intrusion and thermal water-freshwater. At both sites, the water temperature was above 32 °C (Tables 1 and 2).

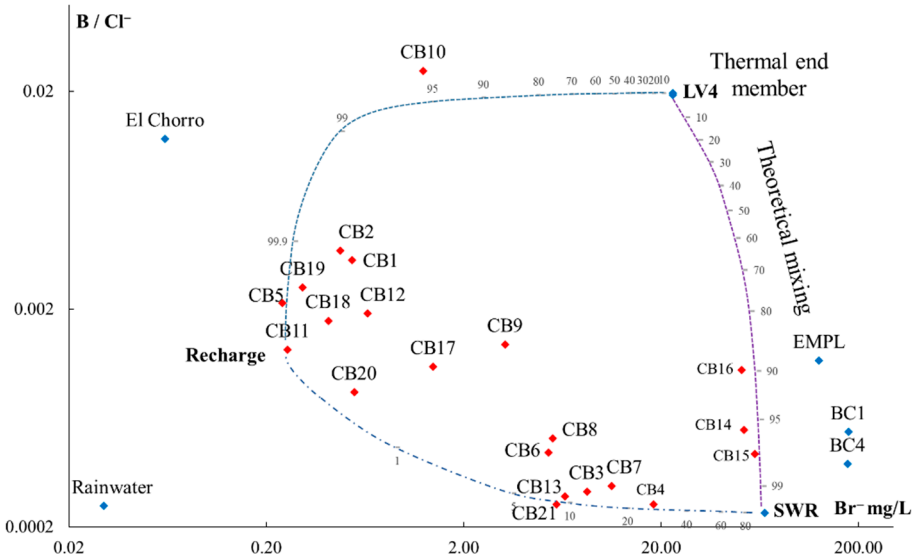

Figure 9. Br^- and B/Cl^- ratio for samples at Bahia Concepcion and their relationship with the end-members LV4 [79], seawater (SWR) [73], Recharge [34], theoretical end member (EMPL) [36].

Regarding the eastern margin of the bay (Figure 1), thermal evidence was not observed from the expected differences between water-air temperature, neither from the chemical characteristics in the Br^-/Cl^- and B/Cl^- relationship (Figure 7). However, it is notorious that there is a water–rock interaction (Figure 9) where the Br^- vs. Cl^- relationship increases due to the probable interaction of halides from volcanic rocks [78,84]; these samples correspond to those located in the Concepción Peninsula, which would also denote the water-rock interaction derived from the existence of a lower topographic slope from the upper part of the basin towards the discharge area, which delays the residence period of the water in the rock, as well as its distance between these. The foregoing allows the conclusion that the origin of the salinity is primarily of meteoric origin, with a signature of seawater in the aforementioned contexts, and the mixture of these with seawater intrusion and thermal water; therefore, it may be possible to determine that the analyzed samples present waters little altered by salinity from the thermal system, maintaining their signature of origin to a certain degree. This is in agreement with Villanueva-Estrada et al. [41] who defined a mixture of two-phase fluids, a primary mixture in the recharge and a secondary in the mixture with the thermal end member, for intertidal and submarine springs. Based on its relative temperatures, several sites would not fall into the category of thermal water, due to the arid climate of the Baja California Peninsula, although their hydro-chemical composition indicates clear influence through hydro-thermalism (the B/Cl^- ratio was especially useful, as anthropogenic impact of boron in the study area can be negligible). This type of water can be named Masked Geothermal Water MGW and would correspond to the sites CB1, CB4, CB5, CB6, and CB19 with a B/Cl^- ratio above 0.007.

5.3. Geothermal Water and Geothermometry

High salinity in thermal springs affects the calculation of reservoir temperatures through geothermometers [67,80]. Especially, the seawater fraction modifies not only the cation ratios, but also the SiO_2 concentration; therefore, in this study, corrected reservoir temperatures were calculated without the seawater component (Table 4, Figure 10). For that purpose, a mixing model was constructed, based on four end-members (SWR [73], CB11, EMPL [34], and LV4 [79]), explaining the composition of the five thermal springs (CB2, CB3, CB14, CB15, CB16). As multiple combinations are possible, the chosen model seeks the simplest explanation, in agreement with the Br^-/Cl^- and B/Cl^- diagram (Figure 7), which indicates the strong influence of seawater on CB14, CB15 and CB16. The model

considers the concentration of Cl^- as the main benchmark; furthermore, Na^+, Mg^{2+}, and SiO_2 were taken into account to find the proportions of each member, respectively.

Table 4. Results from the mixing model and seawater exclusion. Ionic concentration in mg/L.

Sample	EMPL [1] (%)	LV4 [2] (%)	SWR [3] (%)	CB11 [4] (%)	Original Data				Seawater Excluded			
					Na^+	K^+	Mg^{2+}	SiO_2	Na^+	K^+	Mg^{2+}	SiO_2
CB2	99.1	0.6	0	0.4	112	4	15	79	65	8	22	83
CB3	84.4	0	4	11.6	615	32	236	122	717	65	20	128
CB14	16.5	0	72	11.5	7225	446	404	75	2357	213	14	243
CB15	6.5	0	83.5	10	8150	455	519	79	3455	313	9	319
CB16	20.5	0	62.5	17	7100	521	276	212	2595	235	13	259
EMPL [1]	-	-	-	-	5543.3	502.5	0.07 *	463.3	-	-	-	-
LV4 [2]	-	-	-	-	3484	603	0.07	484	-	-	-	-
SWR [3]	-	-	-	-	10,780	399	1280	6	-	-	-	-
CB11 [4]	-	-	-	-	44.5	4	22.6	80	-	-	-	-

* Mg^{2+} from Las Vírgenes geothermal field. [1] Deep thermal seawater, [2] Deep thermal freshwater, [3] Seawater reference, [4] Local recharge water.

Original and corrected data were used to construct ternary Na^+-K^+-Mg^{2+} diagrams and a Cl^--SiO_2 plot, as well as to employ a SiO_2 geothermometer [67] to obtain the equilibrium reservoir temperatures in the Bahía Concepción region.

The ternary Na^+-K^+-Mg^{2+} diagram [70,89], with the influence of seawater (Figure 10a), shows that intertidal thermal springs fall into the partial equilibria field indicating an equilibrium temperature between 190 and 210 °C, while sites CB2 and CB3 correspond to immature water. In contrast, after the effect of seawater was removed (Figure 10b), intertidal thermal springs moved closer toward the equilibrium line, indicating a homogeneous temperature of 220 °C, which is equal to that calculated for the EMPL. CB3 shift closed to the partial equilibria field.

On the other hand, when seawater is removed, a substantial increase (up to six times) of the SiO_2 concentration was observed (Figure 11). This fact led to a more reliable estimation of the equilibrium reservoir temperature, applying the SiO_2 geothermometer.

According to the data from the SiO_2 geothermometer (Table 5), two groups of geothermal sites can be distinguished. One group, formed by the intertidal thermal springs, showed a wider interval of temperature (108 to 175 °C) without the correction for seawater. Conversely, removing the seawater effect led to an increase (and a narrower range) in the calculated temperature (186 to 209 °C), which is close to the obtained temperature in the Na^+-K^+-Mg^{2+} diagram. The second group (CB2 and CB3) is little affected by seawater correction. Slightly lower temperatures (151–188 °C) were calculated by Prol-Ledesma et al. [36] for submarine thermal springs in Bahia Concepción. The obtained temperatures from SiO_2 geothermometers are also similar to the results from different geothermal sites, such as Aysen, Chile [9] Doña Juana, Colombia [90], Java Island [91], South Island, New Zealand [92], and Simao, China [93].

Table 5. Surface and equilibrium reservoir temperatures, based on a SiO_2 geothermometer. After Arnórsson [67].

Site	Surface Temperature (°C)	Equilibrium Reservoir Temperature	
		Original Data	Seawater Excluded
CB2	36.4	112	114.1
CB3	32.7	137	140.3
CB14	53.4	108	186.6
CB15	42.1	110	209.9
CB16	58.6	175	191.9

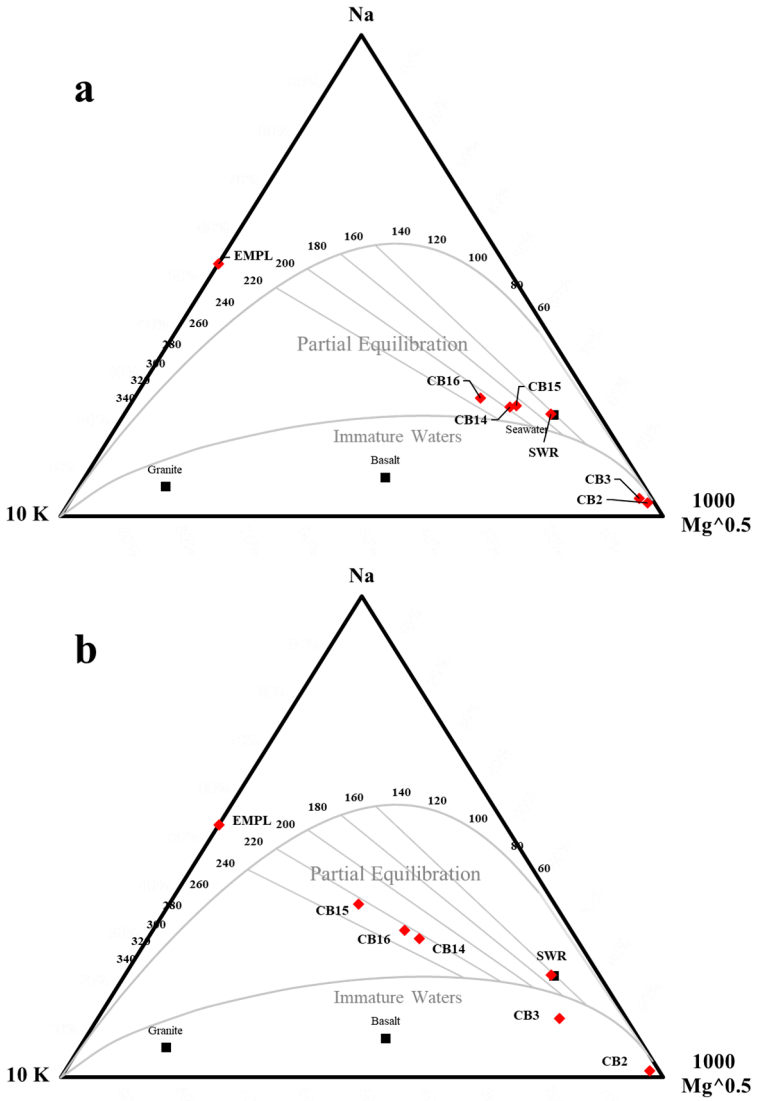

Figure 10. (**a**,**b**) Na^+-K^+-Mg^{2+} diagram [89] with the location of the thermal springs.

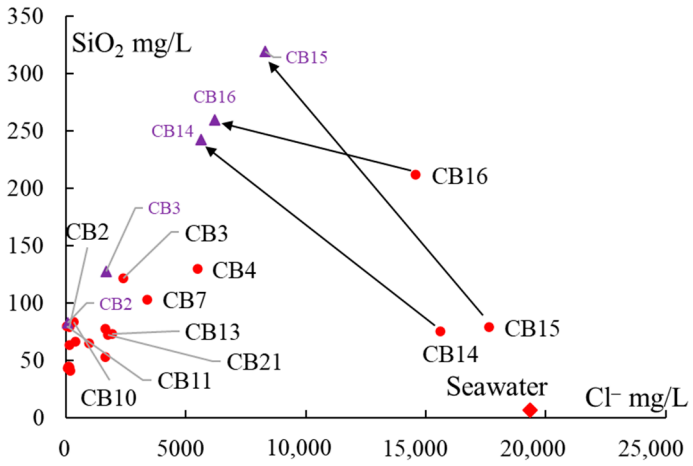

Figure 11. Relationships between Cl^- vs. SiO_2 in groundwater in the Bahía Concepcion watershed.

Due to the small extension of the hydrological watershed and its geological-structural characteristics, it is assumed that at least two levels of groundwater flow occur (Figure 12):

(a) a shallow flow system (Groundwater Shallow level (GWSL)) of rapid circulation in the porous aquifer, constituted by sedimentary deposits in streams and alluvial terraces, in which a short period of residence time between recharge and discharge towards the coastline is presumed [78]; (b) a deeper infiltrated flow system (Groundwater deep level (GWDL)), related to structural discontinuities that affect volcanic and volcanoclastic rocks, generating significant secondary permeability. The geothermal system in depth mainly receives seawater inflows [36]. This recharge occurs when the main faults cross the seabed, providing more seawater influence; Prol-Ledesma et al. [36] and Santos et al. [94] have evidenced a dilution of seawater in the submarine vents of the area. Heated seawater is considered a significant source of submarine groundwater discharges (SGD), involving relevant geochemical processes such as nutrients and pollutants transport [95,96]. Nevertheless, novel findings herein documented indicate the important role meteoric water plays in the recharge of the deep thermal reservoir.

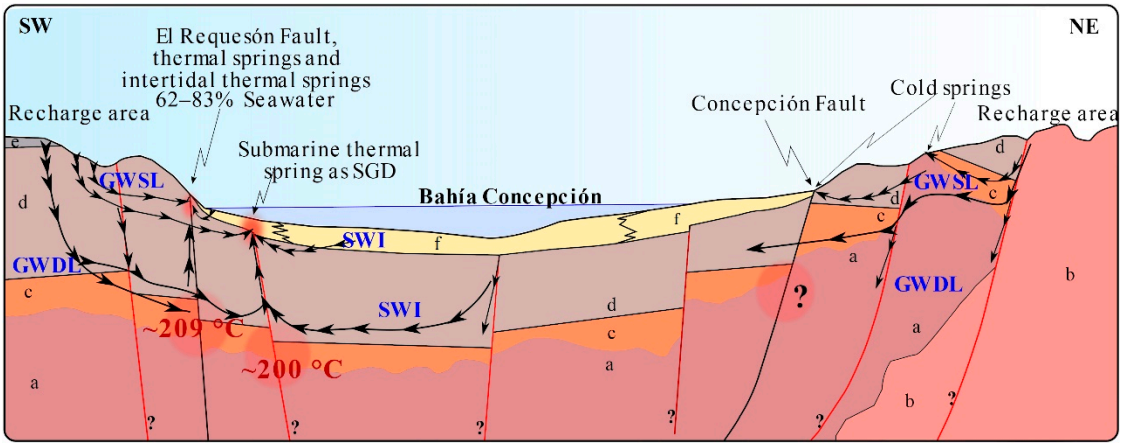

Figure 12. Schematic representation of hydrogeological and geothermal conceptualization at Bahia Concepción. The graphic has not been escalated. Black arrows indicate groundwater flow. Letters corresponding to: (a) Cretaceous granitic basement; (b) Tertiary granitic; (c) Tertiary El Salto Formation; (d) Tertiary Comondú Group; (e) Quaternary basaltic-andesite flows; (f) Quaternary alluvial and marine sediments. After [36,43,46].

The participation of a high saline thermal end-member in the geothermal system of Bahía Concepción was previously proposed by Villanueva-Estrada et al. [41]; however, the mixing relationships found in this study did not show any evidence for this. In contrast, the existence of a probable deep thermal freshwater end-member was inferred, in agreement with Prol-Ledesma et al. [36].

6. Conclusions

The results obtained explain important processes involved in the mixing of groundwater in contact with seawater, e.g., water–rock interaction, rainwater effects. The use of B/Cl^- and Br^-/Cl^- relationships, coupled with hydro-geochemistry and geo-thermometry, allowed the recognition of five MGW in the coastal area of Bahía Concepción (sites CB1, CB4, CB5, CB6, and CB19). It is proposed to apply this methodology in other coastal areas with geo-thermalism of low enthalpy, in order to evaluate potential environmental impacts. Seawater represents the most common origin of salinity (up to 83%) in the coastal thermal spring of Bahía Concepción. Even, sites far from the coastline showed the common Br^-/Cl^- ratio of seawater, due to local rainfalls that incorporate aerosols and spray water droplets from the sea. Thermal springs in the study area are associated with the El Requesón fault, which is the main tectonic structure on the western margin. Geothermal springs related to the Concepción fault were not found; however, the occurrence of MGW indicates the presence of hydro-thermalism. The temperature in the deep geothermal reservoir varies from 114 to 209 °C. This research contributes to an increase

in knowledge of geothermal resources, improving their future use and management in a sustainable framework.

Author Contributions: Conceptualization, P.H.-M. and J.W.; methodology, P.H.-M.; investigation, P.H.-M., J.W., C.G.-R.; resources, J.W., C.G.-R., D.M.; writing—original draft preparation, P.H.-M.; writing—review and editing, P.H.-M., J.W., C.G.-R., D.M.; funding acquisition, C.G.-R., D.M. All authors have read and agreed to the published version of the manuscript.

Funding: The authors acknowledge the resources granted for this research as a part of the projects DGAPA-UNAM-PAPIIT IN110716 and CEGA-FONDAP 15090013.

Institutional Review Board Statement: Not applicable.

Informed Consent Statement: Not applicable.

Data Availability Statement: Not applicable.

Acknowledgments: The authors acknowledge to CONACYT (Mexican science and technology national council) scholarship No. 593495, also the Chilean Agency for International Development Cooperation (AGCID) for the international scholarship granted and to the ANID-Fondap Project 15090013 "Centro de Excelencia en Geotermia de los Andes (CEGA)". The work was also financed by the Programa de Apoyo a Proyectos de Investigación e Innovación Tecnológica from Universidad Nacional Autónoma de México (PAPIIT IN110716). Further, we would like to thank Verónica Rodríguez (CEGA-Laboratory). Thanks to Daniela Alvarado and Raquel Gutiérrez for assistance in fieldwork. Special thanks to the reviewers.

Conflicts of Interest: The authors declare no conflict of interest.

References

1. Chepeliev, M.; Van der Mensbrugghe, D. Global fossil-fuel subsidy reform and Paris Agreement. *Energy Econ.* **2020**, *85*, 104598. [CrossRef]
2. Sayed, E.T.; Wilberforce, T.; Elsaid, K.; Rabaia, M.K.H.; Abdelkareem, M.A.; Chae, K.J.; Olabi, A.G. A critical review on Environmental Impacts of Renewable Energy Systems and Mitigation Strategies: Wind, Hydro, Biomass and Geothermal. *Sci. Total Environ.* **2020**, *766*, 144505. [CrossRef] [PubMed]
3. Boguniewicz-Zabłocka, J.; Łukasiewicz, E.; Guida, D. Analysis of the Sustainable Use of Geothermal Waters and Future Development Possibilities—A Case Study from the Opole Region, Poland. *Sustainability* **2019**, *11*, 6730. [CrossRef]
4. Griebler, C.; Brielmann, H.; Haberer, C.M.; Kaschuba, S.; Kellermann, C.; Stumpp, C.; Hegler, F.; Kuntz, D.; Walker-Hertkorn, S.; Lueders, T. Potential impacts of geothermal energy use and storage of heat on groundwater quality, biodiversity, and ecosystem processes. *Environ. Earth Sci.* **2016**, *75*, 1391. [CrossRef]
5. IRENA. *Renewable Power Generation Costs in 2019*; International Renewable Energy Agency: Abu Dhabi, United Arab Emirates. Available online: https://www.irena.org/publications/2020/Jun/Renewable-Power-Costs-in-2019?fbclid=IwAR3UsYNJqcZta8YxP_VrXkYIIkHmK8f7Xt-_yMOExI29RH9coTRvpksMwP0 (accessed on 2 August 2020).
6. Arango-Galván, C.; Prol-Ledesma, R.M.; Torres-Vera, M.A. Geothermal prospects in the Baja California peninsula. *Geothermics* **2015**, *55*, 39–57. [CrossRef]
7. Carbajal-Martínez, D.; Peiffer, L.; Hinojosa-Corona, A.; Trasviña-Castro, A.; Arregui-Ojeda, S.M.; Carranza-Chávez, F.J.; Flores-Luna, C.; Méndez-Alonzo, R.; Inguaggiato, I.; Casallas-Moreno, K.L. UAV-based thermal imaging and heat output estimation of a coastal geothermal resource: La Jolla beach, Baja California, Mexico. *Renew. Energy* **2021**, *168*, 1364–1376. [CrossRef]
8. Liu, M.; Guo, Q.; Wu, G.; Guo, W.; She, W.; Yan, W. Boron geochemistry of the geothermal waters from two typical hydrothermal systems in Southern Tibet (China): Daggyai and Quzhuomu. *Geothermics* **2019**, *82*, 190–202. [CrossRef]
9. Negri, A.; Daniele, L.; Aravena, D.; Muñoz, M.; Delgado, A.; Morata, D. Decoding fjord water contribution and geochemical processes in the Aysen thermal springs (Southern Patagonia, Chile). *J. Geochem. Explor.* **2018**, *185*, 1–13. [CrossRef]
10. Lund, J.W.; Toth, A.N. Direct utilization of geothermal energy 2020 worldwide review. *Geothermics* **2021**, *90*, 101915. [CrossRef]
11. Muffler, P.; Cataldi, R. Methods for regional assessment of geothermal resources. *Geothermics* **1978**, *7*, 53–89. [CrossRef]
12. Towler, B.F. Geothermal energy. In *The Future of Energy*; Elsevier: Amsterdam, The Netherlands, 2014; p. 390. [CrossRef]
13. Esteller, M.V.; Martínez-Florentino, A.K.; Morales-Reyes, G.P.; Cardona, A.; Expósito, J.L. Mixing processes between thermal waters and non-thermal waters: A case study in Mexico. *Environ. Earth Sci.* **2019**, *78*, 295. [CrossRef]
14. Kaasalainen, H.; Stefánsson, A.; Giroud, N.; Arnórsson, S. The geochemistry of trace elements in geothermal fluids, Iceland. *Appl. Geochem.* **2015**, *62*, 207–223. [CrossRef]
15. Navarro, A.; Font, X.; Viladevall, M. Geochemistry and groundwater contamination in the La Selva geothermal system (Girona, Northeast Spain). *Geothermics* **2011**, *40*, 275–285. [CrossRef]

16. Tomaszewska, B.; Bundschuh, J.; Pająk, L.; Dendys, M.; Delgado-Quezada, V.; Bodzek, M.; Armienta, M.A.; Ormachea-Muñoz, M.; Kasztelewicz, A. Use of low enthalpy and waste geothermal energy sources to solve arsenic problems in freshwater production in selected regions of Latin America using a process membrane distillation—Research into model solutions. *Sci. Total Environ.* **2020**, *714*, 136853. [CrossRef]
17. Wang, X.; Dan, Z.; Cui, X.; Zhang, R.; Zhou, S.; Wenga, T.; Yan, B.; Chen, G.; Zhang, Q.; Zhong, L. Contamination, ecological and health risks of trace elements in soil of landfill and geothermal sites in Tibet. *Sci. Total Environ.* **2020**, *715*, 136639. [CrossRef] [PubMed]
18. Webster, J.G.; Nordstrom, D.K. Geothermal Arsenic. In *Arsenic in Ground Water*; Welch, A.H., Stollenwerk, K.G., Eds.; Springer: Boston, MA, USA, 2003; pp. 101–125. [CrossRef]
19. D'Amore, F.; Arnórsson, S. Geothermal manifestations and hydrothermal alteration. In *Isotopic and Chemical Techniques in Geothermal Exploration, Development and Use: Sampling Methods, Data Handling, Interpretation*; Arnórsson, S., Ed.; IAEA: Vienna, Austria, 2000; pp. 73–83. Available online: https://www.iaea.org/publications/5733/isotopic-and-chemical-techniques-in-geothermal-exploration-development-and-use-sampling-methods-data-handling-interpretation-edited-by-stefan-arnorsson (accessed on 17 August 2019).
20. Prol-Ledesma, R.M. *El Calor de la Tierra*, 3rd ed.; FCE: Mexico City, Mexico; SEP: Mexico City, Mexico; CONACyT: Mexico City, Mexico, 2002; p. 99.
21. Afsin, M.; Allen, D.M.; Kirste, D.; Durukan, U.G.; Gurel; A. ; Oruc, O. Mixing processes in hydrothermal spring systems and implications for interpreting geochemical data: A case study in the Cappadocia region of Turkey. *Hydrogeol. J.* **2014**, *22*, 7–23. [CrossRef]
22. Amiri, V.; Nakhaei, M.; Lak, R.; Kholghi, M. Assessment of seasonal groundwater quality and potential saltwater intrusion: A study case in Urmia coastal aquifer (NW Iran) using the groundwater quality index (GQI) and hydrochemical facies evolution diagram (HFE-D). *Stoch. Environ. Res. Risk Assess.* **2016**, *30*, 1473–1484. [CrossRef]
23. Arnórsson, S. The use of mixing models and chemical geothermometers for estimating underground temperatures in geothermal systems. *J. Volc. Geotherm. Res.* **1985**, *23*, 299–335. [CrossRef]
24. Arnorsson, S.; Stefansson, A.; Bjarnason, J.O. Fluid-Fluid Interactions in Geothermal Systems. *Rev. Mineral. Geochem.* **2007**, *65*, 259–312. [CrossRef]
25. Besser, H.; Mokadem, N.; Redhaounia, B.; Hadji, R.; Hamad, A.; Hamed, Y. Groundwater mixing and geochemical assessment of low-enthalpy resources in the geothermal field of southwestern Tunisia. *Euro-Mediterr. J. Environ. Integr.* **2018**, *3*, 16. [CrossRef]
26. Liu, Y.; Jiao, J.J.; Liang, W.; Kuang, X. Hydrogeochemical characteristics in coastal groundwater mixing zone. *Appl. Geochem.* **2017**, *85*, 49–60. [CrossRef]
27. Trezzi, G.; Garcia-Orellana, J.; Rodellas, V.; Santos-Echeandia, J.; Tovar-Sánchez, A.; Garcia-Solsona, E.; Masqué, P. Submarine groundwater discharge: A significant source of dissolved trace metals to the North Western Mediterranean Sea. *Mar. Chem.* **2016**, *186*, 90–100. [CrossRef]
28. Bertani, R. Geothermal power generation in the world 2010–2014 update report. *Geothermics* **2016**, *60*, 31–43. [CrossRef]
29. Gutiérrez-Negrín, L.C.A.; Canchola-Félix, I.; Romo-Jones, J.M.; Quijano-León, J.L. Geothermal Energy in Mexico: Update and Perspectives. In Proceedings of the World Geothermal Congress 2020, Reykjavik, Iceland, 26 April–2 May 2020.
30. Prol-Ledesma, R.M.; Torres-Vera, M.A.; Rodolfo-Metalpa, R.; Angeles, C.; Lechuga-Deveze, C.H.; Villanueva-Estrada, R.E.; Shumilin, E.; Robinson, C. High heat flow and ocean acidification at a nascent rift in the northern Gulf of California. *Nat. Commun.* **2013**, *4*, 1388. [CrossRef]
31. Prol-Ledesma, R.M.; Moran-Centeno, D.J. Heat flow and geothermal provinces in Mexico. *Geothermics* **2019**, *78*, 183–200. [CrossRef]
32. Leal-Acosta, M.L.; Prol-Ledesma, R.M. Caracterización geoquímica de las manifestaciones termales intermareales de Bahía Concepción en la Península de Baja California. *Bol. Soc. Geol. Mex.* **2016**, *68*, 395–407. [CrossRef]
33. López-Sánchez, A.; Báncora-Alsina, C.; Prol-Ledesma, R.M.; Hiriart, G. A new geothermal resource in Los Cabos, Baja California Sur, México. In Proceedings of the 28th New Zealand Geothermal Workshop, Auckland, New Zealand, 16–17 November 2006; University of Auckland: Auckland, New Zealand, 2006; pp. S3–S6. Available online: https://www.geothermal-energy.org/pdf/IGAstandard/NZGW/2006/PDF/S3.pdf (accessed on 22 April 2019).
34. Hernández-Morales, P.; Wurl, J. Hydrogeochemical characterization of the thermal springs in northeastern of Los Cabos Block, Baja California Sur, México. *Environ. Sci. Pollut. Res.* **2017**, *24*, 13184–13202. [CrossRef] [PubMed]
35. Portugal, E.; Birkle, P.; Tello, E.; Tello, M. Hydrochemical–isotopic and hydrogeological conceptual model of the Las Tres Vírgenes geothermal field, Baja California Sur, México. *J. Volcanol. Geotherm. Res.* **2000**, *101*, 223–244. [CrossRef]
36. Prol-Ledesma, R.M.; Canet, C.; Torres-Vera, M.A.; Forrest, M.J.; Armienta, M.A. Vent fluid chemistry in Bahía Concepción coastal submarine hydrothermal system, Baja California Sur, Mexico. *J. Volcanol. Geotherm. Res.* **2004**, *137*, 311–328. [CrossRef]
37. Verma, S.P.; Pandarinath, K.; Santoyo, E.; González-Partida, E.; Torres-Alvarado, I.S.; Tello-Hinojosa, E. Fluid chemistry and temperaturas prior to exploitation at the Las Tres Vírgenes geothermal field, México. *Geothermics* **2006**, *35*, 156–180. [CrossRef]
38. Wurl, J.; Rodríguez, L.M.; Cassassuce, F.; Gutiérrez, G.M.; Velázquez, E.R. Geothermal water in the San Juan Bautista Londó aquifer, BCS, Mexico. *Procedia Earth Planet. Sci.* **2013**, *7*, 900–903. [CrossRef]

39. Canet, C.; Prol-Ledesma, R.M.; Proenza, J.A.; Rubio-Ramos, M.A.; Forrest, M.J.; Torres-Vera, M.A.; Rodríguez-Díaz, A.A. Mn-Ba-Hg mineralization at shallow submarine hydrothermal vents in Bahía Concepción, Baja California Sur, Mexico. *Chem. Geol.* **2005**, *224*, 96–112. [CrossRef]
40. Leal-Acosta, M.L.; Shumilin, E.; Mirlean, N.; Lounejeva-Baturina, E.; Sánchez-Rodríguez, I.; Delgadillo-Hinojosa, F.; Borges-Souza, J. Intertidal geothermal hot springs as a source of trace elements to the coastal zone: A case study from Bahía Concepción, Gulf of California. *Mar. Pollut. Bull.* **2018**, *128*, 51–64. [CrossRef]
41. Villanueva-Estrada, R.E.; Prol-Ledesma, R.M.; Rodríguez-Díaz, A.A.; Canet, C.; Torres-Alvarado, I.S.; González-Partida, E. Geochemical processes in an active shallow submarine hydrothermal system, Bahía Concepción, México: Mixing or boiling? *Int. Geol. Rev.* **2012**, *54*, 907–919. [CrossRef]
42. Duque-Trujillo, J.; Ferrari, L.; Orozco-Esquivel, T.; López-Martínez, M.; Lonsdale, P.; Bryan, S.E.; Kluesner, J.; Piñero-Lajas, D.; Solari, L. Timing of rifting in the southern Gulf of California and its conjugate margins: Insights from the plutonic record. *Geol. Soc. Am. Bull.* **2015**, *127*, 702–736. [CrossRef]
43. McFall, C.C. *Reconnaissance Geology of the Concepcíon Bay Area, Baja California, Mexico*; Stanford University Publications in Geological Sciences: Stanford, CA, USA, 1968; Volume 10, pp. 1–25.
44. SGM. *Carta Geológica-Minera y Geoquímica de Loreto G12-5, Escala 1:250000*; Servicio Geológico Mexicano, Secretaria de Economia: Pachuca, Mexico, 2002.
45. Ledesma-Vázquez, J.; Johnson, M.E. Miocene-Pleistocene Tectono-Sedimentary Evolution of Bahía Concepción Region, Baja California Sur (Mexico). *Sediment. Geol.* **2001**, *144*, 83–96. [CrossRef]
46. Durán-Calderón, J.I. Estratigrafía regional y significado tectónico del Grupo Comondú en Baja California Sur, México. Tesis de Maestría, Universidad Nacional Autónoma de México, Mexico City, Mexico, 2016; p. 193.
47. Umhoefer, P.; Dorsey, R.; Willsey, S.; Mayer, L.; Renne, P. Stratigraphy and geochronology of the Comondu group near Loreto, Baja California Sur, Mexico. *Sediment. Geol.* **2001**, *144*, 125–147. [CrossRef]
48. Ferrari, L.; Orozco-Esquivel, T.; Bryan, S.E.; López-Martínez, M.; Silva-Fragoso, A. Cenozoic magmatism and extension in western Mexico: Linking the Sierra Madre Occidental silicic large igneous province and the Comondú Group with the Gulf of California rift. *Earth Sci. Rev.* **2018**, *183*, 115–152. [CrossRef]
49. Johnson, M.E.; Ledesma-Vázquez, J.; Mayall, M.A.; Minch, J. Upper Pliocene stratigraphy and depositional systems: The Peninsula Concepción Basin in Baja California Sur, Mexico. In *Pliocene Carbonates and Related Facies Flanking the Gulf of California, Mexico*; Johnson, M.E., Ledesma-Vázquez, J., Eds.; Geological Society of America: Boulder, CO, USA, 1997; Volume 318, pp. 57–72. [CrossRef]
50. Ledesma-Vázquez, J.; Johnson, M.E.; Gutiérrez-Sanchez, S. El Mono chert: A shallow-water chert from the Pliocene Infierno Formation, Baja California Sur, Mexico. In *Pliocene Carbonates and Related Facies Flanking the Gulf of California, Mexico*; Johnson, M.E., Ledesma-Vázquez, J., Eds.; Geological Society of America: Boulder, CO, USA, 1997; Volume 318, pp. 73–81. Available online: https://pubs.geoscienceworld.org/books/chapter-pdf/966928/i0-8137-2318-3-318-0-73.pdf (accessed on 7 June 2019).
51. Hausback, B.P. Cenozoic volcanic and tectonic evolution of Baja California Sur, Mexico. In *Geology of the Baja California Peninsula: Pacific Section*; Frizzel, V.A., Jr., Ed.; Society Economic Paleontologist and Mineralogist: Tulsa, OK, USA, 1984; Volume 39, pp. 219–236.
52. Martín-Barajas, A. Vulcanism and extension of the extensional province of the gulf of California. *Bol. Soc. Geol. Mex.* **2000**, *53*, 72–83. [CrossRef]
53. Sawlan, M.G.; Smith, J.G. Petrologic characteristics, age and tectonic setting of Neogene volcanic rocks in northern Baja California Sur, Mexico. In *Geology of the Baja California Peninsula*; Pacific Section; Frizzell, A.V., Ed.; Society of Economic Paleontologists and Mineralogists: Tulsa, OK, USA, 1984; Volume 39, pp. 237–251. Available online: http://archives.datapages.com/data/pac_sepm/055/055001/pdfs/237.htm (accessed on 3 October 2018).
54. Umhoefer, P.J.; Mayer, L.; Dorsey, R.J. Evolution of the margin of the Gulf of California near Loreto, Baja California Peninsula, Mexico. *Geol. Soc. Am. Bull.* **2002**, *114*, 849–868. [CrossRef]
55. Drake, W.R.; Umhoefer, P.J.; Griffiths, A.; Vlad, A.; Peters, L.; McIntosh, W. Tectono-stratigraphic evolution of the Comondú Group from Bahía de La Paz to Loreto, Baja California Sur, Mexico. *Tectonophysics* **2017**, *719–720*, 107–134. [CrossRef]
56. Sutherland, F.H.; Kent, G.M.; Harding, A.J.; Umhoefer, P.J.; Driscoll, N.W.; Lizarralde, D.; Fletcher, J.M.; Axen, G.J.; Holbrook, W.S.; González-Fernández, A.; et al. Middle Miocene to early Pliocene oblique extension in the southern Gulf of California. *Geosphere* **2012**, *8*, 752–770. [CrossRef]
57. Forrest, M.J.; Ledesma-Vázquez, J.; Ussler, W., III; Kulongoski, J.T.; Hilton, D.R.; Greene, H.G. Gas geochemistry of a shallow submarine hydrothermal vent associated with El Requesón fault zone in Bahía Concepción, Baja California Sur, México. *Chem. Geol.* **2005**, *224*, 82–95. [CrossRef]
58. CONAGUA. *Estadísticas del Agua en México*; Comisión Nacional del Agua: Mexico City, Mexico, 2018; p. 303. Available online: http://sina.conagua.gob.mx/publicaciones/EAM_2018.pdf (accessed on 19 December 2020).
59. CLICOM. Daily Weather Data from SMN Through its Web Platform CICESE. Available online: http://clicom-mex.cicese.mx/ (accessed on 8 December 2017).
60. CONAGUA. *Actualización de la Disponibilidad de Agua en el Acuífero Bahía Concepción (0331), Estado de Baja California Sur*; Reporte Técnico; Comisión Nacional del Agua: Mexico City, Mexico, 2020; p. 24. Available online: https://sigagis.conagua.gob.mx/gas1/Edos_Acuiferos_18/BajaCaliforniaSur/DR_0331.pdf (accessed on 12 December 2020).

61. Camprubí, A.; Canet, C.; Rodríguez-Diaz, A.A.; Prol-Ledesma, R.M.; Blanco-Florido, D.; Villanueva, R.E.; López-Sánchez, A. Geology, ore deposits and hydrothermal venting in Bahia Concepcion, Baja California Sur, Mexico. *Island Arc* **2008**, *17*, 6–25. [CrossRef]
62. Leal-Acosta, M.L.; Shumilin, E.; Mirlean, N.; Delgadillo-Hinojosa, F.; Sánchez- Rodríguez, I. The impact of marine shallow-water hydrothermal venting on arsenic and mercury accumulation by seaweeds Sargassum sinicola in Concepcion Bay, Gulf of California. *Environ. Sci. Process Impacts* **2013**, *15*, 470–477. [CrossRef]
63. Estradas-Romero, A.; Prol-Ledesma, R.M.; Zamudio-Reséndiz, M.E. Relación de las características geoquímicas de fluidos hidrotermales con la abundancia y riqueza de especies del fitoplancton de Bahía Concepción, Baja California Sur, México. *Bol. Soc. Geol. Mex.* **2009**, *61*, 87–96. Available online: http://www.scielo.org.mx/scielo.php?script=sci_arttext&pid=S1405-33222009000100009&lng=es&nrm=iso (accessed on 22 September 2017). [CrossRef]
64. Melwani, A.; Kim, S. Benthic infaunal distributions in shallow hydrothermal vent sediments. *Acta Oecol.* **2008**, *33*, 162–175. [CrossRef]
65. Arnórsson, S.; D'Amore, F. Sampling of geothermal fluids: On-site measurements and sample treatment. In *Isotopic and Chemical Techniques in Geothermal Exploration, Development and Use: Sampling Methods, Data Handling, Interpretation*; Arnórsson, S., Ed.; IAEA: Vienna, Austria, 2000; pp. 84–142. Available online: https://www.iaea.org/publications/5733/isotopic-and-chemical-techniques-in-geothermal-exploration-development-and-use-sampling-methods-data-handling-interpretation-edited-by-stefan-arnorsson (accessed on 17 August 2019).
66. Vengosh, A. Salinization and saline environments. In *Treatise on Geochemistry*; Holland, H.D., Turekian, K.K., Eds.; Elsevier Ltd.: Amsterdam, The Netherlands, 2003; Volume 9, pp. 333–365. [CrossRef]
67. Arnórsson, S. *Isotopic and Chemical Techniques in Geothermal Exploration, Development and Use: Sampling Methods, Data Handling, Interpretation*; IAEA: Vienna, Austria, 2000; p. 351. Available online: https://www.iaea.org/publications/5733/isotopic-and-chemical-techniques-in-geothermal-exploration-development-and-use-sampling-methods-data-handling-interpretation-edited-by-stefan-arnorsson (accessed on 17 August 2019).
68. Verma, S.P.; Pandarinath, K.; Santoyo, E. SolGeo: A new computer program for solute geothermometers and its application to Mexican geothermal fields. *Geothermics* **2008**, *37*, 597–621. [CrossRef]
69. Piper, A.M. A graphic procedure in the geochemical interpretation of water-analyses. *Eos Trans. Am. Geophys. Union* **1944**, *25*, 914–928. [CrossRef]
70. Powell, T.; Cumming, W. Spreadsheets for geothermal water and gas geochemistry. Proceedings of Thirty-Fifth Workshop on Geothermal Reservoir Engineering, Stanford, CA, USA, 1–3 February 2010. Available online: https://earthsciences.stanford.edu/ERE/pdf/IGAstandard/SGW/2010/powell.pdf (accessed on 5 January 2019).
71. Birkle, P.; Portugal Marín, E.; Pinti, D.L.; Clara Castro, M. Origin and evolution of geothermal fluids from Las Tres Vírgenes and Cerro Prieto fields, Mexico—Co-genetic volcanic activity and paleoclimatic constraints. *J. Appl. Geochem.* **2016**, *65*, 36–53. [CrossRef]
72. Tomaszkiewicz, M.; Abou Najm, M.; El-Fadel, M. Development of a groundwater quality index for seawater intrusion in coastal aquifers. *Environ. Model. Softw.* **2014**, *57*, 13–26. [CrossRef]
73. Nozaki, Y. Elemental Distribution: Overview. In *Encyclopedia of Ocean Sciences*, 2nd ed.; Steele, J.H., Ed.; Elsevier: Amsterdam, The Netherlands, 2008; Volume 2, pp. 840–845. [CrossRef]
74. Parkhurst, D.L.; Appelo, C.A.J. Chapter A43. In *Description of Input and Examples for PHREEQC Version 3—A Computer Program for Speciation, Batch-Reaction, One-Dimensional Transport, and Inverse Geochemical Calculations: US Geological Survey Techniques and Methods*; US Department of the Interior: Washington, DC, USA, 2013; p. 497. Available online: http://pubs.usgs.gov/tm/06/a43 (accessed on 14 November 2020).
75. Custodio, E.; Herrera, C. Utilización de la relación Cl/Br como trazador hidrogeoquímico en hidrología subterránea. *Bol. Geol. Min.* **2000**, *111*, 49–67.
76. Vengoechea, A.M.; Rojano, R.E.; Arregoces, H.A. Dispersion and Concentration of PM 10 Particles in a Caribbean Coastal City. *Inf. Tecnol.* **2018**, *29*, 123–130. [CrossRef]
77. Alcalá, F.J.; Custodio, E. Using the Cl/Br ratio as a tracer to identify the origin of salinity in aquifers in Spain and Portugal. *J. Hydrol.* **2008**, *359*, 189–207. [CrossRef]
78. Mendoza-Salgado, R.; Lechuga-Deveze, C.; Ortega-Rubio, A. First approach of a method to assess water quality for arid climate bay in the Gulf of California. *Sci. Total Environ.* **2005**, *347*, 208–216. [CrossRef] [PubMed]
79. Tello-Hinojosa, E.; Verma, M.P.; González-Partida, E. Geochemical characteristics of reservoir fluids in the Las Tres Virgenes, BCS, Mexico. In Proceedings of the World Geothermal Congress 2005, Antalya, Turkey, 24–29 April 2005.
80. Nicholson, K. *Geothermal Fluids Chemistry and Exploration Techniques*; Springer: Berlin/Heidelberg, Germany, 1993; p. 255. [CrossRef]
81. Farhadian Babadi, M.; Mehrabi, B.; Tassi, F.; Cabassi, J.; Pecchioni, E.; Shakeri, A.; Vaselli, O. Geochemistry of fluids discharged from mud volcanoes in SE Caspian Sea (Gorgan Plain, Iran). *Int. Geol. Rev.* **2020**, 1–16. [CrossRef]
82. Engle, M.A.; Doolan, C.A.; Pitman, J.A.; Varonka, M.S.; Chenault, J.; Orem, W.H.; McMahon, P.B.; Jubb, A.M. Origin and geochemistry of formation waters from the lower Eagle Ford Group, Gulf Coast Basin, south central Texas. *Chem. Geol.* **2020**, *550*, 119754. [CrossRef]

83. Lipiec, I.; Wątor, K.; Kmiecik, E. The application of selected hydrochemical indicators in the interpretation of hydrogeochemical data—A case study from Busko-Zdrój and Solec-Zdrój (Poland). *Ecol. Indic.* **2020**, *117*, 106460. [CrossRef]
84. Stefánsson, A.; Arnórsson, S.; Sveinbjörnsdóttir, Á.E.; Heinemaier, J.; Kristmannsdóttir, H. Isotope (δd, δ18o, 3h, δ13c, 14c) and chemical (B, Cl) Constrains on water origin, mixing, water-rock interaction and age of low-temperature geothermal water. *Appl. Geochem.* **2019**, *108*, 104380. [CrossRef]
85. Arnórsson, S.; Andrésdóttir, A. Processes controlling the distribution of boron and chlorine in natural waters in Iceland. *GCA* **1995**, *59*, 4125–4146. [CrossRef]
86. Lgourna, Z.; Warner, N.; Bouchaou, L.; Boutaleb, S.; Hssaisoune, M.; Tagma, T.; Ettayfi, N.; Vengosh, A. Elucidating the sources and mechanisms of groundwater salinization in the Ziz Basin of southeastern Morocco. *Environ. Earth Sci.* **2014**, *73*, 77–93. [CrossRef]
87. Hao, Y.; Pang, Z.; Kong, Y.; Tian, J.; Wang, Y.; Liao, D.; Fan, Y. Chemical and isotopic constraints on the origin of saline waters from a hot spring in the eastern coastal area of China. *Hydrogeol. J.* **2020**, *28*, 2457–2475. [CrossRef]
88. Sekuła, K.; Rusiniak, P.; Wątor, K.; Kmiecik, E. Hydrogeochemistry and Related Processes Controlling the Formation of the Chemical Composition of Thermal Water in Podhale Trough, Poland. *Energies* **2020**, *13*, 5584. [CrossRef]
89. Giggenbach, W.F. Chemical techniques in geothermal exploration. In *Guidebook: Application of Geochemistry in Resources Development*; UNITAR/UNDP: Geneva, Switzerland, 1991; pp. 119–144.
90. Gómez Diaz, E.; Marín Cerón, M.I. Hydrogeochemical characteristics at Doña Juana Complex (SW Colombia): A new area for geothermal exploration in the Northern Andes region. *Geothermics* **2019**, 101738. [CrossRef]
91. Purnomo, B.J.; Pichler, T. Geothermal systems on the island of Java, Indonesia. *J. Volcanol. Geotherm.* **2014**, *285*, 47–59. [CrossRef]
92. Reyes, A.G.; Christenson, B.W.; Faure, K. Sources of solutes and heat in low-enthalpy mineral waters and their relation to tectonic setting, New Zealand. *J. Volcanol. Geotherm.* **2010**, *192*, 117–141. [CrossRef]
93. Zhang, Y.; Zhou, X.; Liu, H.; Yu, M.; Hai, K.; Tan, M.; Huo, D. Hydrogeochemistry, Geothermometry, and Genesis of the Hot Springs in the Simao Basin in Southwestern China. *Geofluids* **2019**, 1–23. [CrossRef]
94. Santos, I.R.; Lechuga-Deveze, C.; Peterson, R.; Burnett, W. Tracing submarine hydrothermal inputs into a coastal bay in Baja California using radon. *Chem. Geol.* **2011**, *282*, 1–10. [CrossRef]
95. Burnett, W.C.; Taniguchi, M.; Oberdorfer, J. Measurement and significance of the direct discharge of groundwater into the coastal zone. *J. Sea Res.* **2001**, *46*, 109–116. [CrossRef]
96. Dimova, N.; Ganguli, P.M.; Swarzenski, P.W.; Izbicki, J.A.; O'Leary, D. Hydrogeologic controls on chemical transport at Malibu Lagoon, CA: Implications for land to sea exchange in coastal lagoon systems. *J. Hydrol. Reg. Stud.* **2017**, *11*, 219–233. [CrossRef]